Published in final edited form as:
Proteins. 2012 April ; 80(4): 1143–1153. doi:10.1002/prot.24015.

Molecular basis of the Fructose-2,6-bisphosphatase reaction of PFKFB3: Transition state and the C-terminal function

Michael C. Cavalier[1], **Song-Gun Kim**[2], **David Neau**[3], and **Yong-Hwan Lee**[1,*]

[1]Department of Biological Sciences, Louisiana State University, Baton Rouge LA 70803, USA

[2]Korea Research Institute of Bioscience and Biotechnology, Daejeon 305-806, Korea

[3]NE-CAT, Cornell University, Argonne IL 60439, USA

Abstract

The molecular basis of Fructose-2,6-bisphosphatase (F-2,6-P_2ase) of 6-phosphofructo-2-kinase/fructose-2,6-bisphosphatase (PFKFB) was investigated using the crystal structures of the human inducible form (PFKFB3) in a phospho-enzyme intermediate state (PFKFB3-P•F-6-P), in a transition state-analogous complex (PFKFB3•AlF_4), and in a complex with pyrophosphate (PFKFB3•PP_i) at resolutions of 2.45Å, 2.2Å, and 2.3Å, respectively. Trapping the PFKFB3-P•F-6-P intermediate was achieved by flash cooling the crystal during the reaction, and the PFKFB3•AlF_4 and PFKFB3•PP_i complexes were obtained by soaking. The PFKFB3•AlF_4 and PFKFB3•PP_i complexes resulted in removing F-6-P from the catalytic pocket. With these structures, the structures of the Michaelis complex and the transition state were extrapolated. For both the PFKFB3-P formation and break down, the phosphoryl donor and the acceptor are located within ~5.1Å, and the pivotal point 2-P is on the same line, suggesting an “in-line” transfer with a direct inversion of phosphate configuration. The geometry suggests that NE2 of His253 undergoes a nucleophilic attack to form a covalent N-P bond, breaking the 2O-P bond in the substrate. The resulting high reactivity of the leaving group, 2O of F-6-P, is neutralized by a proton donated by Glu322. Negative charges on the equatorial oxygens of the transient bipyramidal phosphorane formed during the transfer are stabilized by Arg252, His387, and Asn259. The C-terminal domain (residues 440–446) was rearranged in PFKFB3•PP_i, implying that this domain plays a critical role in binding of substrate to and release of product from the F-2,6-P_2ase catalytic pocket. These findings provide a new insight into the understanding of the phosphoryl transfer reaction.

Keywords

x-ray crystallography; glycolysis; catalysis; transition state; conformation

Introduction

Fructose-2,6-bisphosphate (F-2,6-P_2) is known to be the most potent allosteric activator of the rate-limiting enzyme in glycolysis, 6-phosphofructose-1-kinase (PFK-1), as well as an inhibitor of the gluconeogenic enzyme fructose-1,6-bisphosphatase (F-1,6-P_2ase). As such, this small signaling molecule allows for switching between the two pathways of glucose metabolism within the liver, playing a crucial role in maintaining glucose homeostasis in mammalian bodies and controlling the rates of glycolysis in other tissues[1]. The concentration of F-2,6-P_2 is regulated by the bifunctional enzyme, 6-phosphofructo-2-

*To whom correspondence should be addressed; Y-HL, Louisiana State University, Department of Biological Sciences, 531 Choppin Hall, Baton Rouge, LA 70803. Phone (225) 578-0522, Fax (225) 578-7258, yhlee@lsu.edu..

kinase/fructose-2,6-bisphosphatase (PFKFB). The N-terminal half of the enzyme subunit (6-phosphofructo-2-kinase domain) catalyzes the synthesis of F-2,6-P_2, using fructose-6-phosphate (F-6-P) and adenosine 5'-triphosphate (ATP) as substrates (Figure 1A). Conversely, the C-terminal half (fructose-2,6-bisphosphatase domain) is responsible for the hydrolytic degradation of F-2,6-P_2 into F-6-P and inorganic phosphate (P_i). These two mutually opposing catalytic activities are controlled by different mechanisms such that either activity is predominant in a given physiological condition. Ultimately, the PFKFB control of F-2,6-P_2 production/degradation controls the rate of glucose metabolism[2].

In order to optimize the regulation of F-2,6-P_2 in a tissue-specific manner, there exist four PFKFB tissue-specific isoforms each encoded by separate genes *pfkfb1–4*. They are liver, PFKFB1; heart, PFKFB2; testis, PFKFB4; and inducible forms, PFKFB3[3; 4; 5; 6]. These isoforms share highly conserved core catalytic domains (85%)(Figure 2), but differ greatly in their kinetic properties and responses to regulatory signals. These differences are mostly due to highly divergent N- and C-terminal regulatory domains[7; 8; 9]; however, a few but significant sequence differences in the catalytic domains that constitute the secondary residue shells surrounding the active sites also contribute to the kinetic differences[10]. Differences in the structure/function relationships between these isoforms have been addressed using the available crystal structures of PFKFB1, PFKFB3, and PFKFB4[11; 12; 13]. For a more complete comparison, the structure of PFKFB2 needs to be determined.

Unlike the other isoforms, PFKFB3 is ubiquitously expressed upon the onset of hypoxia[14; 15] and has been shown to be identical to the isoforms isolated from placenta, pancreatic β-islet, and brain[10; 16; 17]. PFKFB3 has a uniquely large 6-phosphofructo-2-kinase to fructose-2,6-bisphosphatase activity ratio compared to other isoforms. This isoform, which has a native activity ratio of roughly 700 fold kinase-to-phosphatase activity, dramatically increases up to 3000 upon phosphorylation of Ser460 by protein kinase A (PKA) or AMP-dependent protein kinase (AMPPK)[18; 19; 20; 21; 22]. Recent studies suggest that this form is a causative molecule of highly elevated levels glycolysis in tumor cells, a phenomenon known as the `Warburg effect'[23]. Thus, it has also been suggested that PFKFB3 may serve as a promising new target for future cancer chemotherapy[24; 25]. Consequently, an intensive study to investigate the structure/function relationship of PFKFB3 has been performed, and the catalytic mechanism of the kinase reaction for the synthesis of F-2,6-P_2 was recently hypothesized from the structural evidence[11; 26].

The low bisphosphatase activity of PFKFB3, which is lower than that of other isoforms by an order of magnitude[19], provides a unique opportunity for the study of the bisphosphatase reaction. In the present study, we determined an improved crystal structure of the PFKFB3 phospho-enzyme intermediate state (PFKFB3-P•F-6-P) trapped during the bisphosphatase reaction; PFKFB3 complexed with aluminum tetrafluoride (AlF_4) within the bisphosphatase catalytic pocket (PFKFB3•AlF_4), which mimics the transition state of a phosphoryl transfer; and PFKFB3 complexed with inorganic pyrophosphate (PFKFB3•PP_i) in which a novel conformation of C-terminus residues 440–446 was observed. From these structures, we were able to deduce all the structures necessary for understanding of this reaction, namely, the Michaelis complex state and the transition states. This study provided a new insight into the catalytic mechanism of this histidine phosphatase and the results are discussed here.

Results

Overall Structure

In this study, three models (PFKFB3-P•F-6-P, PFKFB3•AlF_4, and PFKFB3•PP_i) which in concert detail the enzyme state through substrate binding, catalysis, and product release during the bisphosphatase reaction (Schematic 1) are being introduced. The global

conformation of these models including crystal contacts, the dimeric interface, and domain/domain interactions are not significantly affected by the liganding conditions varied in this experiment. As detailed in previous structural studies, a subunit of the active dimer of PFKFB3 is comprised of a single polypeptide encompassing two catalytic domains. (Figure 1A) In each complex, N-terminal residues 4 through 15 form a β-hairpin structure to make contacts with bisphosphatase domain at the area where the residues involved in binding of both product and substrate are concentrated. In this way, the self-regulatory effect of the N-terminus on F-2,6-P_2ase activity[11] is not affected by experimentally varied liganding. Unlike the N-terminus, the C-terminus residues (460–520) remain disordered and have not yet been elucidated. The only apparent conformational change observed occurs at C-terminus residues 440–446 and is explained in detail in later sections of this article.

PFKFB3-P•F-6-P Structure

The electron densities of the crystals soaked with F-2,6-P_2 show F-2,6-P_2 to be dephosphorylated to F-6-P within the catalytic pocket of the bisphosphatase domain. The phosphate transferred from O2 of F-2,6-P_2 was covalently bound to NE2 of His253 with a distance of 1.7Å in a covalent phospho-enzyme intermediate state (PFKFB3-P•F-6-P). The distance between the His-P phosphorous and O2 of F-6-P, the leaving group, is 3.4Å. The oxygens of the His-P phosphate make numerous interactions with the protein residues such that the E-P state is stabilized. The residues involved in the interactions with the E-P phosphate are Arg252, His387, and Asn259. The details of these interactions are described in following sections, and they are summarized in Table I. The improved PFKFB3-P•F-6-P model described here is an extension of resolution and confirms the orientation previously described by PDB ID:2I1V[26]. A similar model of PFKFB in the E-P•F-6-P intermediate state has been previously described using the rat liver isoform (RL2K) of PFKFB[27]. Unfortunately, conclusions regarding the human PFKFB3 should be drawn cautiously from the RL2K model, as this was a truncated form, which lacked the kinase domain and thirty residues of the C-terminus. As a result, the bound F-6-P was found near the interface of two protein molecules within the crystal lattice, and the water-bridged interactions between the analogous Thr440 and F-6-P, whose importance is described in later sections, was lost. These circumstances resulted in a notably different position of F-6-P[27; 28].

PFKFB3•AlF_4 structure

A crystal soaked with NaF and $AlCl_3$ shows an electron density representing a square planar AlF_4 within the catalytic pocket of the PFKFB3 bisphosphatase domain (Figure 3A). The metal makes two collinear axial bonds to NE2 of His253 and to the oxygen of a water molecule, each with the distance of 2.1Å and 1.9Å, respectively.

As shown in Figure 3A, F3 interacts with His387, F4 with Asn259 and Arg252, and F2 with Arg252. F1 of AlF_4 makes a unique short-range interaction with Asn256. Geometric details of the interactions are provided in Table I. Consequently, the atoms of bound AlF_4, together with the apical water and NE2 of His253 constitute, a tetragonal bipyramidal structure, which seems to mimic a trigonal bipyramidal phosphorane structure that is transiently formed during the phosphoryl transfer reaction. The apical water molecule also makes a short-range, 2.8Å, interaction with Glu322. This finding strongly suggests the function of Glu322 is to neutralize the leaving group and to activate the attacking water molecule.

The PFKFB3•AlF_4 structure is the first PFKFB3 model described in which the product of the phosphatase domain, F-6-P, is absent. It is also the first structure in which the invariant region (residues 440–446), whose amino acid sequence and conformation is strongly conserved among all four PFKFB isoforms, is disordered (Figure 3B). Details regarding this particular conformational change will be discussed in the following sections.

PFKFB3•PP_i structure

The crystal soaked with pyrophosphate and F-6-P showed electron density representing pyrophosphate (PP_i) within the bisphosphatase site (Figure 4A), while the kinase site was occupied by two pyrophosphate molecules (data not shown). Within the bisphosphatase domain, the second phosphorous of the pyrophosphate and its conjugate oxygens have a lower occupancy. The high occupancy phosphorus atom is 3.5Å from His253. Although it was included in the soaking solution, F-6-P is absent from the bisphosphatase active site, suggesting that the E•P_i•F-6-P complex is not favored. This model can be taken as a representative of the E•P_i state.

Residues 440–446, which were interpreted as a random coil in all models before the PFKFB3•AlF_4 structure, in which it was disordered (Figure 4C), can now be seen as a weak, continuous density which was interpreted as an α-helix extending outward from the active site (Figure 4C).

Comparison of Bisphosphatase Active Sites

Three models are described above (PFKFB3-P•F-6-P, PFKFB3•AlF_4, and PFKFB3•PP_i). Within each of these three models, a representation of the transferred 2-phosphate (His-P, AlF_4, and PP_i, respectively), each at a various stage of the catalytic reaction (E-P•F-6-P, E-P-F-6-P/E-P-H_2O transition states, and E•P_i, respectively), can be extracted. Within each of these representations, the represented oxygens of the transferred 2-phosphate maintain interactions with His387, Asn259, and Arg252 (Table I). Therefore, these residue side-chains must remain in contact with the 2-phosphate oxygens throughout the reaction.

Glu322 makes interactions with the O2 of F-6-P in the PFKFB3-P•F-6-P model, with the apical water of the bipyramid within the PFKFB3•AlF_4 model, and with the O1 of high occupancy phosphate of PP_i within the PFKFB3•PP_i model (Table I). The significance of this will be explained in later sections.

The O1 oxygen of the high occupancy phosphate of PP_i within the PFKFB3•PP_i model is at the approximately same position as the O2 of F-6-P within the PFKFB3-P•F-6-P model. The summation of the atoms within these two molecules yields a representation of the bisphosphatase substrate F-2,6-P_2 (Figure 5A), allowing a hypothetical model of the Michaelis complex (Figure 5B).

Because of the absence of F-6-P within the PFKFB3•PP_i model, two waters, which bridge extensive interactions between F-6-P and the C-terminus in the PFKFB3-P•F-6-P model, are lost. The Cα of Thr440 moves 2.5Å out of the active site, and the side-chain rotates 113–132° outward from the active site. Simultaneously, His441 acts to replace Arg442 in a π-Cation interaction with Tyr333. The displacement of Arg442 allows coiling of the newly observed α-helix (Figure 4B).

Degradation of Fructose-2,6-Bisphosphate

Based on the three structures, a molecular model of the F-2,6-P_2ase reaction of the human inducible form of PFKFB is suggested. This mechanism is in direct agreement with the mechanism suggested for the human testes form of PFKFB[28]. The models introduced in this work, in particular PFKFB3•AlF_4, increase confidence in assumptions concerning the mechanism of PFKFB3 by offering structural details that were not previously available in any isoform.

Binding of Substrate (E → E•F-2,6-P_2)—In Figure 5B, the F-2,6-P_2 representation summed from the high occupancy phosphate of the PFKFB3•PP_i model and the F-6-P of the

PFKFB3-P•F-6-P model confirms that the 6-phosphate moiety is recognized by Arg347, Lys351, and Tyr362 and that the 2-phosphate moiety is recognized by residues His387, Asn259, and Arg252. The C-terminal residues 440–446 are stabilized as a random coil through water-mediated interactions with F-2,6-P_2.

Formation of the Phospho-Enzyme Intermediate (E•F-2,6-P_2 → E-P•F-6-P)—In Figure 5C, the three newly introduced models allow us to observe three positions of the 2-phosphate during the phosphoryl transfer; PP_i, AlF_4, and His-P. By tracking through all three representations of the phosphorous of 2-phosphate (His-P, AlF_4, PP_i), a nearly straight line punctuated at the ends by the NE2 of His253 and the O2 of F-6-P can be seen, suggesting an "inline" transfer mechanism[2]. This supports the direct inversion of oxygen stereochemistry through the PFKFB3-P•F-6-P to PFKFB3•PP_i models with the transition state represented by the equatorial plane formed by the peripheral fluorines of AlF_4. An equatorial plane created by the migrating peripheral oxygens of phosphate was hypothesized[28], but never before has it been so clearly depicted. Note that the arrangement of AlF_4, bound by PFKFB3, cannot exactly mimic the trigonal bipyramidal transition state of the phosphoryl-transfer reaction but is considered an adequate approximation in phosphoryl-transfer mechanisms[29; 30; 31; 32; 33].

Upon binding of F-2,6-P_2, the NE2 of His253 is in position for a nucleophilic attack on the 2-phosphate. This attack is aided by the interactions of 2-phosphate with Arg252, His387, and Asn259. The resulting interactions would stabilize the transition state by delocalizing the electrons in the 2-phosphate towards the side-chains of residues Arg252, His387, and Asn259 making the phosphorous of the 2-phosphate more electrophilic. This would enhance the nucleophilic attack of the lone pair of electrons of the NE2 of His253. The removal of 2-phosphate from F-2,6-P_2 would leave a highly basic anion that would need to be neutralized to prevent reformation of the reaction substrates. The general proximity of Glu322 suggests that it is positioned to function as the general acid and donates a proton to the leaving O2 after His-P formation. This is consistent with kinetic studies of the conserved Glu327 within the rat liver isoform, which suggests that Glu327 acts as both a general acid during the E-P formation and a general base during E-P breakdown[2; 34]. The reaction mechanism resulting in the E-P•F-6-P intermediate is summarized in Schematic 2.

Release of F-6-P and Degradation of the Phospho-Histidine Intermediate (E-P•F-6-P → E-P → E•P_i)—Upon the departure of the F-6-P and the two waters which bridge interactions between F-6-P and residues 440–446, this segment of the C-terminus is no longer stabilized as a random coil. A molecule of water would then move in to the apex of a tetragonal bipyramidal configuration and the mechanism by which E-P would breakdown is presumably the reverse of its formation. Glu322 would withdraw a hydrogen from the water and the resulting strong anion would attack the electrophilic phosphate while the transition state is stabilized by residues Arg252, His387, and Asn259 (Schematic 2). The importance of the water found at the apex of the bipyramid now becomes immediately apparent. The activation of water by Glu322 has been hypothesized[2; 28; 34], but the placement of a water molecule in a position of attack has never before been depicted. The track of the peripheral oxygens through the equatorial transition state during the formation of free phosphate is also represented by the PFKFB3•AlF_4 model. In actuality, because of the absence of F-6-P in the PFKFB3•AlF_4 model, the track of the peripheral oxygens during the phospho-histidine breakdown is more directly portrayed than the formation of the phospho-histidine. Upon the formation of the free phosphate, residues 440–446 shift away from the active site and appear to coil into an α-helix.

Discussion

The three models introduced in this article provide a clearer understanding of the bisphosphatase reaction of the inducible form of the bifunctional enzyme by both supporting previous assumptions derived from other isoforms, and distinguishing unique characteristics of this particular polypeptide. The PFKFB3-P•F-6-P model allows confirmation of the positioning of the fructose and 6-phosphate atoms as well as the residues responsible for their binding, whereas the PFKFB3•PP_i does the same for the atoms of the 2-phosphate. The PFKFB3•AlF_4 model directly illustrates the stereochemistry of the bisphosphatase reaction for the first time amongst all isoforms.

It has been suggested that the reduced bisphosphatase activity of PFKFB3 is solely due to the presence of a serine at residue 302 instead of an arginine as conserved in the other isoforms (Figure 2). This residue is said to interact with the 2-phosphate and further stabilizes the transitions state, if conserved[11; 12; 13]. Studies have reported that the restoration of this serine to arginine rescues the ability to generate and degrade the His-P intermediate[19]. Strangely, however, despite not a having arginine at position 302, PFKFB3 has the ability to form the phospho-histidine intermediate but merely lacks the ability to degrade it. This article provides structural evidence of a conformational change in C-terminal residues 440–446 and suggests that the reason for the depressed bisphosphatase activity may be more complex than simply a single mutated residue. The absence of F-6-P from the active site causes rearrangement of the C-terminus residues 440–446. Perhaps, this is suggestive that bisphosphatase activity is further regulated through the control of ligand binding and product release, or perhaps the degradation of the active site after the release of F-6-P.

It should be noted that the pivotal residues of this conformational change (Thr440, His441, Arg442) are absolutely conserved across all known mammalian isoforms of fructose-2,6-bisphosphatase. In addition, previous works with the rat liver isoform, which was truncated just before the Thr-His-Arg segment, resulted in a nine-fold increase in k_{cat}, an eleven-fold increase in K_m, and relief of pH dependent regulation of bisphosphatase activity[9].

No similar conformation change in residues 440–446 has been seen in any other isoforms (Figure 1B), yet additional studies are needed to conclusively ensure that this phenomenon is unquestionably unique to PFKFB3. However, from our research, we are confident that the π-cation interaction between Arg442 and Tyr333 is unique to PFKFB3 among all currently known isoforms. In both PFKFB1 and PFKFB4 models, this conserved arginine forms a salt bridge with an aspartic acid, namely Asp353 and Asp351, respectively. Arg442 does not interact with a glutamic acid, Glu348, at this same position within PFKFB3(Figure 2).

Materials and Methods

Preparation and crystallization of PFKFB3

Protein preparation and crystallization was similar to methods previously described[11; 26]. The His^6-tagged human inducible isoform of the bifunctional enzyme, PFKFB3, was expressed in Escherichia coli BL21 (DE3) pLysS and was purified by Ni-NTA affinity columns. The protein sample was further purified using Q-sepharose anion-exchange chromatography. This purified protein was kept at a concentration of 8 mg ml^{-1} in pH 8.0, 20 mM Tris-HCl, 10 mM Na_xP_i, 5 mM β-mercaptoethanol, and 5% glycerol. Crystal were grown using sitting drop vapor diffusion with a 1:1 (v/v) mixture of protein with a mother liquor of 100 mM Tris-HCl, pH 7.5, 20–25% ethylene glycol, 200–400mM Tartaric Acid, 5% glycerol, and 12% polyethylene glycol 4000. Crystals in a size of 0.2 × 0.2 × 0.05 mm were grown in two to three weeks.

The crystals were soaked with cryoprotectant solutions for 0.5 to 2 hours to allow binding of the desired ligands. Cryoprotectant solutions consisted of 20 mM Tris-HCl pH 7.5 buffer and 12% polyethylene glycol 4000, and were enriched with 35% ethylene glycol and the targeted ligands. The PFKFB3-P•F-6-P crystal was soaked with 3mM ADP 0.5mM F-2,6-P_2. The PFKFB3•AlF_4 crystal was soaked with 3mM ADP, 0.5mM F-6-P, 2mM $AlCl_3$, and 8mM NaF. The PFKFB3•PP_i crystal was soaked with 3mM PP_i. The soaked crystals were flash cooled at 100K and the temperature was maintained during data collection using an Oxford cryo device.

Data Collection and Processing

Diffraction data for the PFKFB3•AlF_4 and the PFKFB3-P•F-6-P crystals was collected at The Gulf Coast Consortium Protein Crystallography Beamline (PX1) in The Center for Advanced Microstructures and Devices (CAMD), Louisiana State University, Baton Rouge, LA using a x-ray source wavelength of 1.3808Å the data was recorded on a Mar 165mm CCD detector and was integrated, merged, and scaled using HKL2000[35].

Diffraction data for the PFKFB3•PP_i crystal was collected at The Northeastern Collaborative Access Team (NE-CAT) beamline at the Advanced Photon Source (Argonne National Laboratory) using an x-ray source wavelength of 0.9792Å. The data was recorded on an ADSC Q315 (315mm × 315mm) detector and was integrated, merged, and scaled using HKL2000[35]. Statistics of the diffraction data and structure refinement are summarized in Table II. All crystals belonged to the $P6_522$ space group, and the cell dimensions were similar.

Structure Determination and Refinement

The reduced data was formatted for the program suite of CCP4[36; 37] and 5% of the data was marked for free R-factor measurements in subsequent structure refinements. Initial models of all complexes were determined using REFMAC[38] within the CCP4 suite with the PFKFB3•ADP•EDTA complex (PDB ID: 2AXN[11]) as the starting molecule after removal of the ligand and solvent molecules. The initial model went through many cycles of manual model rebuilding and validation using the program COOT[39]. Binding of the ligands was confirmed, referring to the |Fo| -|Fc| omit maps that were generated, when R_{crys}/R_{free} reached 0.25/0.28 or below and the ligands were incorporated into the complex models.

As summarized in Table II, the PFKFB3-P•F-6-P complex has R_{free}/R_{crys} of 0.247/0.193 using a total of 3,849 scatterers, including solvent molecules, against all 30,381 available reflections in the resolution range of 30.0–2.45Å. The structure contains a total of 441 amino acid residues of the full-length protein of 520 residues. As in the PFKFB3•ADP•EDTA complex, the C-terminus (residues 446–520) is mostly disordered.

The final structure of the PFKFB3•AlF_4 complex has R_{free}/R_{crys} of 0.242/0.200 using a total of 3,837 scatterers, including solvent molecules, against all 38,530 available reflections in the resolution range of 30.0–2.25Å. The structure contains a total of 431 amino acid residues of the full length protein of 520 residues.

The final structure of the PFKFB3•PP_i complex has R_{free}/R_{crys} of 0.236/0.184 using a total of 3,959 scatterers, including solvent molecules, against all 36,888 available reflections in the resolution range of 35.0–2.30Å. The structure contains a total of 439 amino acid residues of the full-length protein, which consists of 520 residues.

The atomic coordinates and structure factors of the **PFKFB3-P•F-6-P** complex (PDB ID: 3QPV), the **PFKFB3•AlF$_4$** complex (PDB ID: 3QPW), and the **PFKFB3•PP$_i$** complex (PDB ID: 3QPU) have been deposited in the RCSB Protein Data Bank.

Acknowledgments

The authors thank Dr. Henry Bellamy at The Center for Advanced Microstructures and Devices, Louisiana State University, Baton Rouge, LA., and the staffs at The Northeastern Collaborative Access Team (NE-CAT) beamline at the Advanced Photon Source (Argonne National Laboratory), Argonne, IL. The authors would also like to thank Blake Crochet and Dr. Joeng-Do Kim for proofreading the manuscript.

Funding: This study has been supported by grants from NIH (1R01 CA124758-01) and Louisiana Board of Regents (LEQSF(2007–10)-RD-A-12) to Y.-H.L.

Abbreviations used

PFKFB	6-phosphofructo-2-kinase/fructose-2,6-bisphosphatase
6-PF-2-K	6-phosphofructo-2-kinase
F-2,6-P_2ase	fructose-2,6-bisphosphatase
PFK-1	6-phosphofructose-1-kinase
F-1,6-P_2ase	fructose-1,6-bisphosphatase
F-2,6-P_2	fructose-2,6-bisphosphate
F-6-P	fructose-6-phosphate
ATP	adenosine 5'-triphosphate
P_i	orthophosphate
PP_i	pyrophosphate
PKA	protein kinase A
AMPPK	AMP-dependent protein kinase
AlF_4	aluminum tetrafluoride

References

1. Claus TH, El-Maghrabi MR, Regen DM, Stewart HB, Mcgrane M, Kountz PD, Nyfeler F, Pilkis J, Pilkis SJ. The Role of Fructose 2,6-Bisphosphate in the Regulation of Carbohydrate-Metabolism. Curr Top Cell Regul. 1984; 23:57–86. [PubMed: 6327193]
2. Kountz PD, Freeman S, Cook AG, El-Maghrabi MR, Knowles JR, Pilkis SJ. The Stereochemical Course of Phospho Group Transfer Catalyzed by Rat-Liver 6-Phosphofructo-2-Kinase. J Biol Chem. 1988; 263:16069–16072. [PubMed: 2972703]
3. Algaier J, Uyeda K. Molecular-Cloning, Sequence-Analysis, and Expression of a Human-Liver Cdna Coding for Fructose-6-P,2-Kinase-Fructose-2,6-Bisphosphatase. Biochem Bioph Res Co. 1988; 153:328–333.
4. Sakai A, Kato M, Fukasawa M, Ishiguro M, Furuya E, Sakakibara R. Cloning of cDNA encoding for a novel isozyme of fructose 6-phosphate,2-kinase/fructose 2,6-bisphosphatase from human placenta. J Biochem. 1996; 119:506–511. [PubMed: 8830046]
5. Heine-Suner D, Diaz-Guillen MA, Lange AJ. Rodriquez De Cordoba S. Sequence and structure of the human 6-phosphofructo-2-kinase/fructose-2,6-bisphosphatase heart isoform gene (PFKFB2). Eur J Biochem. 1998; 254:103–110. [PubMed: 9652401]
6. Manzano A, Rosa JL, Ventura F, Perez JX, Nadal M, Estivill X, Ambrosio S, Gil J, Bartrons R. Molecular cloning, expression, and chromosomal localization of a ubiquitously expressed human 6-phosphofructo-2-kinase/ fructose-2, 6-bisphosphatase gene (PFKFB3). Cytogenet Cell Genet. 1998; 83:214–217. [PubMed: 10072580]
7. Kurland IJ, Li L, Lnage AJ, Correia JJ, El-Maghrabi MR, Pilkis SJ. Regulation of rat 6-phosphofructo-2-kinase/fructose-2,6-bisphosphatase. Role of the NH2-terminal region. J Biol Chem. 1993; 268:14056–14064. [PubMed: 8390983]

8. Kurland IJ, Chapman B, El-Maghrabi MR. N- and C-termini modulate the effects of pH and phosphorylation on hepatic 6-phosphofructo-2-kinase/fructose-2,6-bisphosphatase. Biochem J. 2000; 347:459–467. [PubMed: 10749675]
9. Lin K, Kurland IJ, Li L, Lee YH, Okar D, Marecek JF, Pilkis SJ. Evidence for NH2- and COOH-terminal Interactions in Rat 6-phosphofructo-2-kinase/ Fructose-2,6-bisphosphatase. J Biol Chem. 1994; 269:16953–16960. [PubMed: 8207019]
10. El-Maghrabi MR, Noto F, Wu N, Manes N. 6-phosphofructo-2-kinase/fructose-2,6-bisphosphatase: suiting structure to need, in a family of tissue-specific enzymes. Curr Opin Clin Nutr. 2001; 4:411–418.
11. Kim SG, Manes NP, El-Maghrabi MR, Lee YH. Crystal structure of the hypoxiainducible form of 6-phosphofructo-2-kinase/fructose-2,6-bisphosphatase (PFKFB3) - A possible new target for cancer therapy. Biol Chem. 2006; 281:2939–2944.
12. Hasemann CA, Istvan ES, Uyeda K, Deisenhofer J. The crystal structure of the bifunctional enzyme 6-phosphofructo-2-kinase/fructose-2,6-bisphosphatase reveals distinct domain homologies. Structure. 1996; 4:1017–1029. [PubMed: 8805587]
13. Lee YH, Li Y, Uyeda K, Hasemann CA. Tissue-specific structure/function differentiation of the liver isoform of 6-phosphofructo-2-kinase/fructose-2,6-bisphosphatase. J Biol Chem. 2003; 278:523–530. [PubMed: 12379646]
14. Minchenko A, Leshchinsky I, Opentanova I, Sang NL, Srinivas V, Armstead V, Caro J. Hypoxia-inducible factor-1-mediated expression of the 6-phosphofructo-2-kinase/fructose-2,6-bisphosphatase-3 (PFKFB3) gene - Its possible role in the Warburg effect. J Biol Chem. 2002; 277:6183–6187. [PubMed: 11744734]
15. Minchenko O, Opentanov I, Caro J. Hypoxic regulation of the 6-phosphofructo-2-kinase/fructose-2,6-bisphosphatase gene family (PFKFB-1–4) expression in vivo. Febs Lett. 2003; 554:264–270. [PubMed: 14623077]
16. Sakakibara R, Okudaira T, Fujiwara K, Kato M, Hirata T, Yamanaka S, Naito M, Fukasawa M. Tissue distribution of placenta-type 6-phosphofructo-2-kinase/fructose-2,6-bisphosphatase. Biochem Bioph Res Co. 1999; 257:177–181.
17. Goren N, Manzano A, Riera L, Ambrosio S, Ventura F, Bartrons R. 6-phosphofructo-2-kinase/fructose-2,6-bisphosphatase expression in rat brain during development. Mol Brain Res. 2000; 75:138–142. [PubMed: 10648897]
18. Marsin AS, Bouzin C, Bertrand L, Hue L. The stimulation of glycolysis by hypoxia in activated monocytes is mediated by AMP-activated protein kinase and inducible 6-phosphofructo-2-kinase. J Biol Chem. 2002; 277:30778–30783. [PubMed: 12065600]
19. Manes NP, El-Maghrabi MR. The kinase activity of human brain 6-phosphofructo-2-kinase/fructose-2,6-bisphosphatase is regulated via inhibition by phosphoenolpyruvate. Arch Biochem and Bioph. 2005; 438:125–136.
20. Okamura N, Sakakibara R. A common phosphorylation site for cyclic AMP-dependent protein kinase and protein kinase C in human placental 6-phosphofructo-2-kinase/fructose-2,6-bisphosphatase. Biosci Biotech Bioch. 1998; 62:2039–2042.
21. Marsin AS, Bertrand L, Rider MH, Deprez J, Beauloye C, Vincent MF, Van den Berghe G, Carling D, Hue L. Phosphorylation and activation of heart PFK-2 by AMPK has a role in the stimulation of glycolysis during ischaemia. Curr Biol. 2000; 10:1247–1255. [PubMed: 11069105]
22. Atsumi T, Chesney J, Metz C, Leng L, Donnelly S, Makita Z, Mitchell R, Bucala R. High expression of inducible 6-phosphofructo-2-kinase/fructose-2,6-bisphosphatase (iPFK-2; PFKFB3) in human cancers. Cancer Res. 2002; 62:5881–5887. [PubMed: 12384552]
23. Warburg O. On the origin of cancer cells. Science. 1956; 123:309–14. [PubMed: 13298683]
24. Chesney J, Telang S, Yalcin A, Clem A, Wallis N, Bucala R. Targeted disruption of inducible 6-phosphofructo-2-kinase results in embryonic lethality. Biochem Biophys Res Co. 2005; 331:139–46.
25. Hirata T, Watanabe M, Miura S, Ijichi K, Fukasawa M, Sakakibara R. Inhibition of tumor cell growth by a specific 6-phosphofructo-2-kinase inhibitor, N-bromoacetylethanolamine phosphate, and its analogues. Biosci Biotech Bioch. 2000; 64:2047–2052.

26. Kim SG, Cavalier M, El-Maghrabi MR, Lee YH. A direct substrate-substrate interaction found in the kinase domain of the bifunctional enzyme, 6-phosphofructo-2-kinase/fructose-2,6-bisphosphatase. J Mol Biol. 2007; 370:14–26. [PubMed: 17499765]
27. Lee YH, Olson TW, Ogata CM, Levitt DG, Banaszak LJ, Lange AJ. Crystal structure of a trapped phosphoenzyme during a catalytic reaction. Nat Struct Biol. 1997; 4:615–618. [PubMed: 9253407]
28. Yuen MH, Mizuguchi H, Lee YH, Cook PF, Uyeda K, Hasemann CA. Crystal structure of the H256A mutant of rat testis fructose-6-phosphate,2-kinase/fructose-2,6-bisphosphatase. J Biol Chem. 1999; 274:2176–2184. [PubMed: 9890980]
29. Olesen C, Sorensen TLM, Nielsen RC, Moller JV, Nissen P. Dephosphorylation of the calcium pump coupled to counterion occlusion. Science. 2004; 306:2251–2255. [PubMed: 15618517]
30. Coleman DE, Berghuis AM, Lee E, Linder ME, Gilman AG, Sprang SR. Structures of Active Conformations of G(I-Alpha-1) and the Mechanism of GTP Hydrolysis. Science. 1994; 265:1405–1412. [PubMed: 8073283]
31. Fisher AJ, Smith CA, Thoden JB, Smith R, Sutoh K, Holden HM, Rayment I. X-Ray Structures of the Myosin Motor Domain of Dictyostelium-Discoideum Complexed with Mgadp-Center-Dot-BeFx and Mgadp-Center-Dot-AlF4- Biochemistry. 1995; 34:8960–8972. [PubMed: 7619795]
32. Rittinger K, Walker PA, Eccleston JF, Smerdon SJ, Gamblin SJ. Structure at 1.65 angstrom of RhoA and its GTPase-activating protein in complex with a transition-state analogue. Nature. 1997; 389:758–762. [PubMed: 9338791]
33. Golicnik M. Metallic Fluoride Complexes as Phosphate Analogues for Structural and Mechanistic Studies of Phosphoryl Group Transfer Enzymes. Acta Chim Slov. 2010; 57:272–287.
34. Sakurai M, Hasemann CA, Uyeda K. Activation of Glu325AIa mutant enzyme of fructose 6-phosphate 2-kinase: Fructose 2,6-bisphosphatase by exogenous nucleophiles. Faseb J. 2000; 14:A1523–A1523.
35. Otwinowski Z, Minor W. Processing of X-ray diffraction data collected in oscillation mode. Method Enzymol. 1997; 276:307–326.
36. Bailey S. The CCP4 Suite - Programs for Protein Crystallography. Acta Crystallogr D Biol Crystallogr. 1994; 50:760–763. [PubMed: 15299374]
37. Potterton E, Briggs P, Turkenburg M, Dodson E. A graphical user interface to the CCP4 program suite. Acta Crystallogr D Biol Crystallogr. 2003; 59:1131–1137. [PubMed: 12832755]
38. Vagin AA, Steiner RA, Lebedev AA, Potterton L, McNicholas S, Long F, Murshudov GN. REFMAC5 dictionary: organization of prior chemical knowledge and guidelines for its use. Acta Crystallogr D Biol Crystallogr. 2004; 60:2184–95. [PubMed: 15572771]
39. Emsley P, Cowtan K. Coot: model-building tools for molecular graphics. Acta Crystallogr D Biol Crystallogr. 2004; 60:2126–32. [PubMed: 15572765]

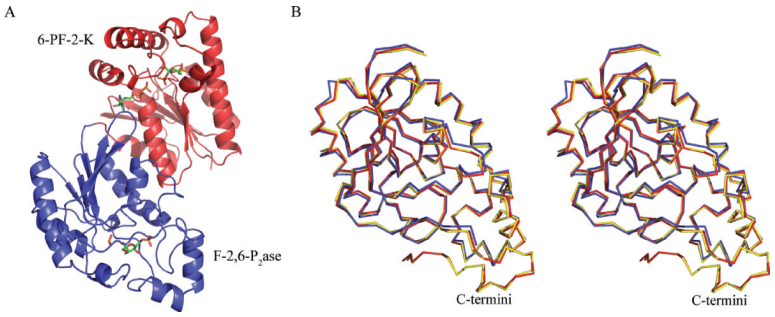

Figure 1. Overall folding of PFKFB3 and sites of ligand binding

All figures, unless otherwise noted, were constructed using PyMOL (The PyMOL Molecular Graphics System, Version 1.2r3pre, Schrödinger, LLC.). **(A)** The overall fold of the monomeric PFKFB3 is represented in a ribbon diagram. The N-terminal kinase domain (6-PF-2-k) is shaded red while the C-terminal bisphosphatase domain (F-2,6-P_2ase) is shaded blue. Each active site location can be discerned by the bound ligands. The ADP and F-2,6-P_2 are within the kinase active site while F-6-P and a covalently attached phosphate are within the bisphosphatase active site. Molecules of interest are represented in stick models. **(B)** To compare the organization of the C-termini, the bisphosphatase domains of the inducible (blue) (PDB ID: 2AXN), testes (yellow) (PDB ID: 1BIF), and liver (red) (PDB ID: 1K6M)[8,9,10] isoforms have been superimposed. The folding patterns are represented by a tracing of the C-alphas.

Figure 2. Sequence alignment of PFKFB

Shown are the sequence alignments of the bisphosphatase domain of the four PFKFB isoforms. Residue numbering coincides with the residues of PFKFB3. Residues involved in catalysis, substrate binding, and the initiation of the conformational change are emphasized with boxes. Asterisks mark residues of interest that are conserved in all isoforms except for PFKFB3.

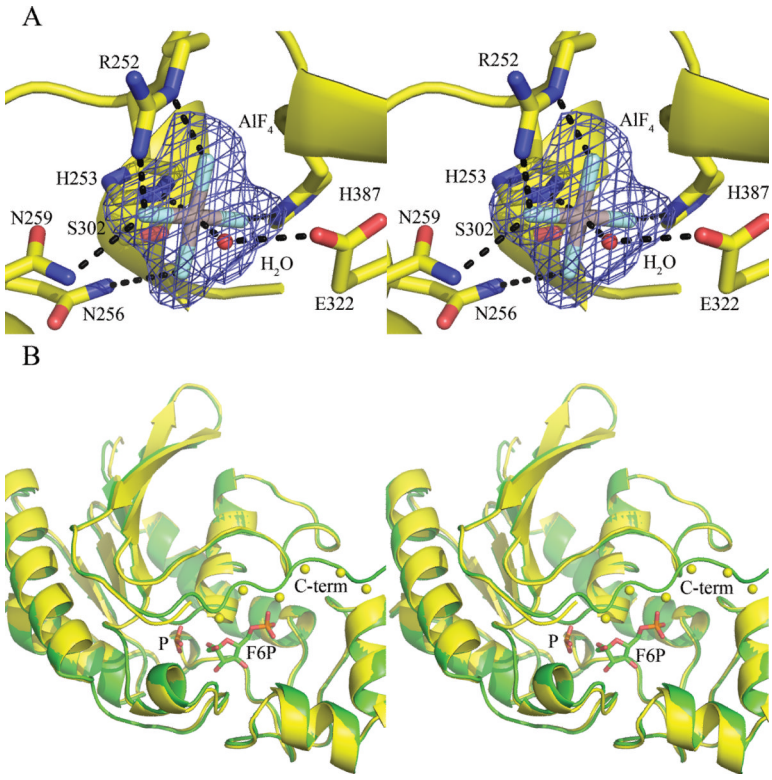

Figure 3. Aluminum tetrafluoride within the active site

(A) A stereo view within the bisphosphatase active site of the **PFKFB3•AlF$_4$** model is shown. The mesh represents the $|F_o|$ -$|F_c|$ electron density omit map of aluminum tetrafluoride and a bound water molecule within the bisphosphatase active site. The map is contoured at 3.0σ levels. Arg252, Asn259, and His387 interact with the peripheral fluorines of aluminum tetrafluoride. Glu322 interacts with a water at the apex of the bipyramidal structure. The aluminum atom is situated 1.9Å from the water and 2.1Å from His253. The dotted lines mark significant interactions. Molecules/residues of interest are represented in stick models. **(B)** Shown is a ribbon representation in stereo view of the overlapping bisphosphatase active sites of the **PFKFB3-P•F-6-P**(green) and **PFKFB3•AlF$_4$**(yellow) models. C-terminal residues 440–446 of the **PFKFB3•AlF$_4$** model can no longer be tracked. Spheres represent the positions of the C-alphas of the missing residues as projected from the **PFKFB3-P•F-6-P** model.

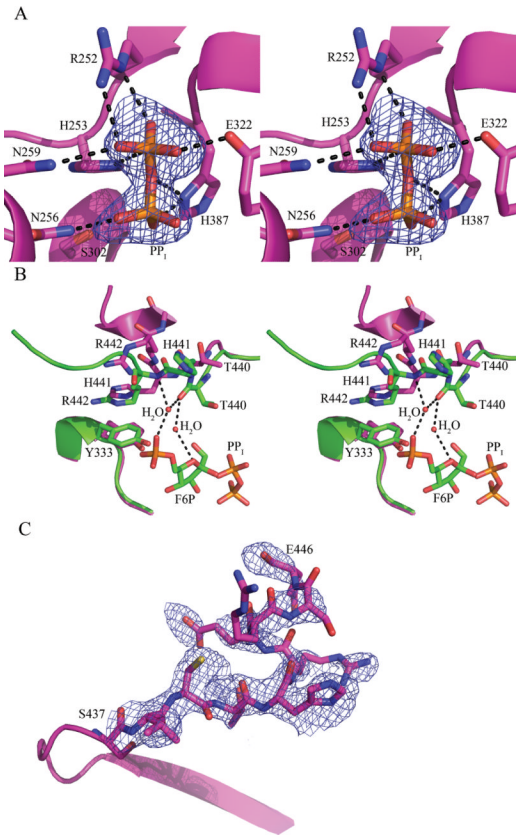

Figure 4. Pyrophosphate within the active site

(A) A stereo view within the bisphosphatase active site of the **PFKFB3•PP$_i$** model is shown. The mesh represents the $|F_o|$ -$|F_c|$ electron density omit map of PP$_i$ within the bisphosphatase active site. The map is contoured at 3.0σ levels. Arg252, Asn259, and His387 interact with the pyrophosphate oxygens that are assumed to be at the positions of the 2-phosphate oxygens of F-2,6-P$_2$. The phosphorous is situated 3.5Å from His235. The dotted lines mark significant interactions. Molecules/residues of interest are represented in stick models. **(B)** Ribbon representations in stereo of the overlapping models of **PFKFB3-P•F-6-P** (green) and **PFKFB3•PP$_i$** (magenta) are shown. Molecules/residues of interest are represented in stick models. Upon the absence of F-6-P, two waters which bridge interactions with the C-terminal segment covering the active site are lost. The C-terminal residues 440–446 are no longer seen as a random coil extending over the bisphosphatase active site, but as a helix extending outwards away from the active site. After the loss of the two water bridged interactions, Thr440 rotates out of the active site. Simultaneously, His441 replaces Arg442 in a π-cation interaction with Tyr333. Arg442 can then commence the coiling of the observed helix. **(C)** Shown are the C-terminal residues of the **PFKFB3•PP$_i$** model. Residues 425–436 are represented as a ribbon while residues 437–446 are represented with sticks. The mesh represents the $|F_o|$ -$|F_c|$ electron density omit map of C-terminal residues 437–446 of the bisphosphatase active site. The map is contoured at 2.0σ levels.

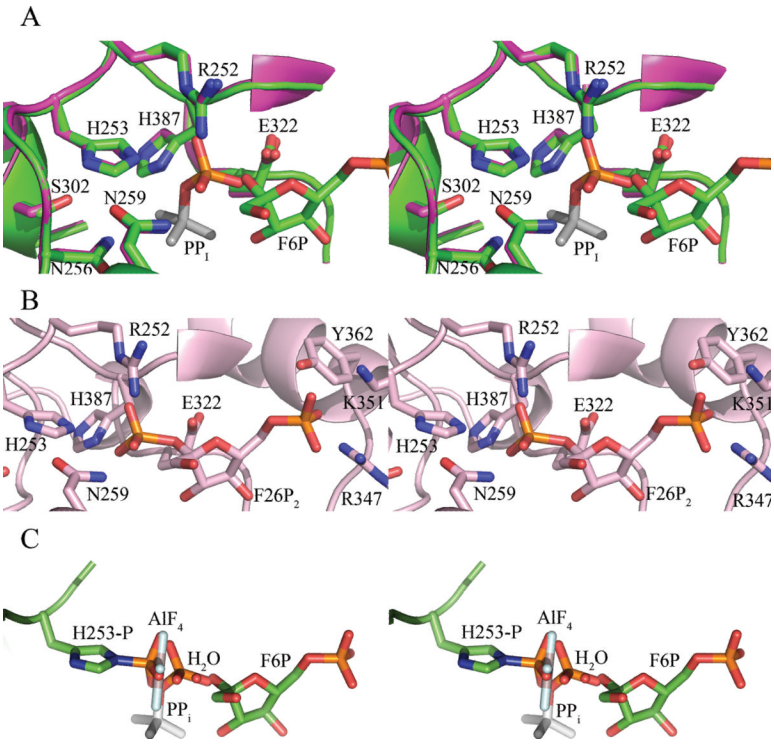

Figure 5. A hypothetical representation of the Michaelis complex (E•F-2,6-P_2)

Here is the Michaelis complex as constructed using ligands from the **PFKFB3-P•F-6-P** and **PFKFB3•PP_i** models. Molecules/residues of interest are represented in stick models. **(A)** A stereo view of the overlapping bisphosphatase active sites of both the **PFKFB3-P•F-6-P**(green) and **PFKFB3•PP_i**(magenta) models is shown. The pyrophosphate of the **PFKFB3•PP_i** model and the F-6-P of the **PFKFB3-P•F-6-P** model have been included but not the covalently bound phosphate. The lower occupancy phosphoryl group of PP_i has been grayed. The remaining ligand atoms can be used to construct a continuous representation of bound F-2,6-P_2. **(B)** A complete representation of the Michaelis complex projection is shown in pink. The 2-phosphate moiety is recognized by residues Arg252, Asn259, and His387. The 6-phosphate moiety is recognized by residues Arg347, Lys351, and Tyr362. **(C)** The ligands from all three models are displayed. The lower occupancy phosphoryl group of PP_i has been grayed. The direct inversion of oxygen stereochemistry, through the E•F-2,6-P_2 to E-P states with the transition state represented by the equatorial plane formed by the peripheral fluorines of AlF_4, can be tracked. By tracking through all three representations of the 2-phosphate phosphorous (His-P, AlF_4, PP_i), one would create an approximately straight line punctuated at the ends by the NE2 of His253 and the O2 of F-6-P.

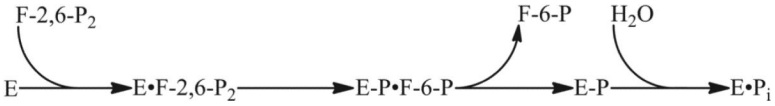

Schematic 1. Schematic 1. The minimal enzymatic reaction

The various enzyme states of PFKFB3 through a minimal enzymatic reaction are shown: free enzyme (E), the Michaelis complex (E•F-2,6-P_2), phospho-enzyme intermediate (E-P•F-6-P), and the states of product release (E-P, E•P_i).

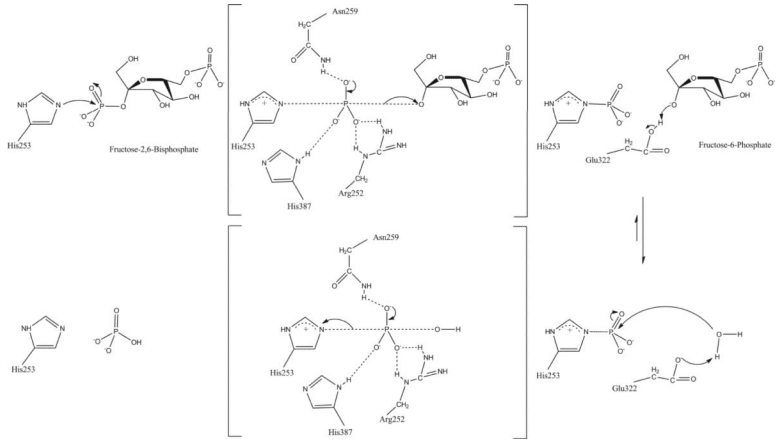

Schematic 2. The complete mechanism of phospho-histidine formation/degradation

This schematic was prepared with ChemBioDraw (ChemBioDraw Ultra 10.0 CambridgeSoft, 100 CambridgePark Drive, Cambridge, MA 02140). Brackets indicate a transition state in which a direct inversion of phosphate stereochemistry occurs. Upon binding of F-2,6-P_2, His253 is in position for a nucleophilic attack on the 2-phosphate. Interactions with Arg252, His387, and Asn259 stabilize the transition state by delocalizing the electrons towards the residues making the P of 2-phosphate more electrophilic. This enhances the nucleophilic attack of the lone pair of electrons of the NE2 of His253. Glu322 acts as a general acid and donates a proton to neutralize the highly basic anion on the first product. Glu322 would then withdraw a hydrogen from a water, and this strong anion would attack the electrophilic phosphate while the transition state is stabilized by residues Arg-252, His-387, and Asn-259 creating the second product.

Table I

Notable interactions between the bisphosphatase active site ligands and the protein.

Protein	Atoms	His-P	AlF_4	PPi	F6P
Arg252	NH1	O1 (3.0)	F4 (2.8)	O4 (3.0)	
		O3 (3.2)	F2 (3.2)	O5 (3.3)	
	NE	O3 (2.9)	F2 (2.7)	O5 (3.0)	
His253	NE2	P (1.7)*	A1 (2.1)	P2 (3.5)	
Asn256	ND2		F1 (3.5)	O3 (3.0)	
Asn259	OD1	O1 (3.1)	F4 (3.0)	O4 (3.0)	
Glu322	OE2			O6 (2.6)	O2 (2.5)
His387	ND1	O2 (2.8)	F3 (2.6)	O (3.3)	
Tyr333	OH				O3P (2.6)
Arg347	NH1				O3P (2.7)
	NH2				O1P (2.9)
Tyr362	OH				O1P (2.5)
Arg392	NH1				O2P (2.6)

Values in parentheses are distances given in angstroms.

*Indicates a covalent bond.

Table II

Statistics of reflection data and structure refinements.

Liganding	**PFKFB3•AlF_4**	**PFKFB3-P•F-6-P**	**PFKFB3•PP_i**
Space group	$P6_522$	$P6_522$	$P6_522$
Unit cell dimension (Å)	102.71 × 102.71 × 257.04	102.15 × 102.15 × 259.44	102.98 × 102.98 × 258.13
Wilson Plot B Value ($Å^2$)	45.7	55.6	41.2
Resolution range (Å)	30.0 – 2.25	30.0 – 2.45	35–2.30
Reflections Observed	351,069	434,030	927,757
Unique Reflections	38,530	30,381	36,888
Reflections R_{free} set	1,951	5,839	1,975
Completeness (%)	99.5 (98.5)	99.6 (98.7)	100 (99.9)
Redundancy	4.7 (4.6)	5.8 (5.7)	7.6 (7.8)
<I/σ>	18.5 (1.8)	14.9 (1.4)	20.0(2.7)
R_{sym}	0.071 (0.462)	0.092 (0.824)	.078 (0.756)
R_{crys}	0.200	0.193	0.184
R_{free}	0.242	0.247	0.236
No. of amino acids	431	441	439
No. of protein atoms	3534	3607	3584
No. of hetero atoms	43	67	55
No. of waters	260	175	320
R.M.S.D. bond lengths (Å)	0.022	0.024	0.024
Angles (°)	1.8	2.2	2.1
Mean B factor			
Protein atoms ($Å^2$)	43.8	42.5	31.2
Hetero atoms ($Å^2$)	51.1	36.5	39.7
Water atoms ($Å^2$)	53.2	48.0	40.4
Ramachandran Outliers(%)	0.0	0.2	0.5
Ramachandran Favored(%)	96.3	93.8	97.2
Poor Rotamers (%)	5.4	8.5	5.3

$R_{sym} = \Sigma_h (\Sigma_j |I_{hj} - \langle I_h \rangle| / \Sigma I_{h,j})$, where h=set of Miller indices, *j*=set of observations of reflection *h*, and $\langle I_h \rangle$=the mean intensity. R.M.S.D. values are deviation from ideal values. $R_{crys} = \Sigma_h ||F_{o,h}| - |F_{c,h}|| / \Sigma_h |F_{o,h}|$. R_{free} was calculated using 5% of the complete data set excluded from refinement. The numbers in parentheses represent values from the highest resolution shell (2.33–2.25 Å for E•AlF_4 complex, 2.54–2.45 Å for the E-P•F-6-P complex, and 2.34–2.30 Å for the E•PP_i complex).